

Revisit the Pitot static tubes in the standards

Yong Moon Choi^a, Yoshiya Terao^b, Noboru Kurihara^b, Aya Iwai^b, Tatsuya Funaki^b, Woong Kang^a, Doan Trang Nguyen^{a,*}

^a Korea Research Institute of Standards and Science, 267 Gajeong-ro, Yuseong-gu, South Korea

^b National Institute of Advanced Industrial Science and Technology, National Metrology Institute of Japan, Tsukuba Central 3, Umezono 1-1-1, Tsukuba, 305-8563, Japan

ARTICLE INFO

Keywords:

Pitot static tube
Reynolds number effect
Pitot tube geometry

ABSTRACT

A Pitot tube is a popular device used for the measurements of flow fields. To control the accuracy of the Pitot tube coefficient, the international standard organization (ISO), the American Society for Testing and Materials (ASTM), and the Japanese Industrial Standards (JIS) issued guidelines that recommended the shape and working conditions of these devices. However, many Pitot tubes on the market do not follow these guidelines. In the present study, various types of Pitot tubes in the market were tested at the National Metrology Institute of Japan (NMIJ) to determine the effects of the geometry and flow characteristics. The results revealed certain limitations in the existing ISO and JIS standards, specifically with regard to the recommended design parameters of the AMCA Pitot tube, the reference coefficient value for the JIS Pitot tube, and the redefinition and limitation of Reynolds numbers pertaining to Pitot tube working conditions.

1. Introduction

In 1732, the Pitot tube was invented and began to be used to determine water flow speeds by Henri Pitot [1]. It was modified and made more accurate and convenient to use by Henry Darcy in 1858 [2]. These improvements established advances in the areas of open-channel and pipe-flow hydraulics [3]. Simultaneously, they played an important role in the development of modern instruments related to impact pressure measurements.

Currently, non-intrusive measurements with optical techniques are popularly used to measure point velocities. However, Pitot tubes are still widely used in fields related to fluid flows. Due to the popularity of Pitot tubes, numerous studies focusing on the characteristics of these devices are conducted with both incompressible and compressible flows. Barker [4] investigated the effects of the viscosity on the accuracy of Pitot tubes. One Pitot tube was mounted in a pipe where the flow underwent streamline motion and with a manometer used to measure the differential pressure according to the mean velocity. Barker [4] defined the region of the fluid velocity in which the Pitot tube adequately complied with the Bernoulli equation as 0.06 m/s. However, Barker [4] did not mention the tube's internal or external diameter when determining the Reynolds number in this research. Macmillan [5] found that the coefficient of a blunt-nosed Pitot tube put in a vertical pipe tended to

increase by approximately 1.5% at Reynolds numbers of less than 50. Moreover, an experiment in that study found that the effect of viscosity depended on the internal diameter of the tube more than the external diameter. Macmillan strongly suggested that Barker used the tube's internal diameter to calculate the Reynolds number.

As commercial software has developed, it has become an effective tool for solving fluid flow models and governing equations. Therefore, with a numerical simulation, Boetcher and Sparrow [6] clarified certain ambiguities with regard to the length dimension definition when the Reynolds number is determined considering Barker's effects and identified quantitatively the threshold Reynolds number at which it is necessary to account for the viscous term. They pointed out that the lower limit of Reynolds number for the Bernoulli interpretation of a Pitot tube as follows: $Re \cong 45$ for a Pitot tube having a hemispherical nosepiece, and $Re \cong 65$ for a Pitot tube having a blunt-faced nosepiece. Spelay et al. [7] provided more detail about the effects of a low Reynolds number on hemispherical-nosepiece Pitot tube measurements in a vertical recirculating pipe loop. They then applied a numerical solution in the experiment using commercial software. The testing fluid was automotive-grade ethylene glycol, and the length scale of the Reynolds number was the Pitot tube's inner diameter. Concurrently, they also reanalyzed the transition Reynolds number data collected from previous studies using the same length scale. The experimental results yielded a transition Reynolds number of $Re \cong 35$, where Bernoulli's equation is

* Corresponding author.

E-mail address: trangnd@kriss.re.kr (D.T. Nguyen).



List of symbols	
C_{HASS}	Corrective coefficient of the high-air-speed system
d	Pitot tube head outer diameter, mm
d_i	Pitot tube head inner diameter, mm
l_{sh}	Length from static holes to the head of the Pitot tube, mm
l_{ss}	Length from static holes to the stem of the Pitot tube, mm
L	Length of the Pitot tube, mm
n	Number of repeated measurements
P	Static pressure in the wind tunnel
r	Pitot tube head outer radius, mm
R_a	Surface roughness of the Pitot tube, μm
Re	Reynolds number
T	Air temperature in the wind tunnel, $^{\circ}\text{C}$
V_p	Air speed measured by the Pitot tube, m/s
V_s	Standard air speed by the reference, m/s
α	Coefficient of the Pitot tube
β	Ratio of the Pitot tube head inner diameter to the outer diameter
γ	Specific heat capacity of air
Δp	Dynamic pressure of the Pitot tube, Pa
Δp_{HASS}	Differential pressure between the nozzle inlet and outlet at the high-air-speed system, Pa
ϵ	expansibility factor
$(1-\epsilon)$	Compressible correction factor
μ	Dynamic viscosity of air, kg/(m.s)
ρ	Density of air, kg/m ³
φ	Humidity in the wind tunnel, %RH

no longer appropriate. This result is also in good agreement with the reanalyzed data of Boetcher and Sparrow [6]. There, transition Reynolds numbers of 28 and 40 were predicted for hemispherical and blunt-faced nosepieces, respectively.

Similar to the effects of the flow similarity, the effects of the shapes of Pitot tubes on their working characteristics have attracted the interest of many researchers. The first investigation related to this topic was done by Ower and Johansen [8] in 1925. They found that geometric parameters of Pitot static tubes, such as the shape of the nose and the distance from the static holes to the stem, affected the pressure distribution parallel with the head and the coefficient of the Pitot tube. In subsequent research on various types of Pitot tubes, Ower and Pankhurst [9] summarized that the calibration factor of Pitot tubes could be considered as 1 at an air velocity greater than 6 m/s. Moreover, at an air velocity of less than 6 m/s, they determined the calibration factors of a hemispherical-nose Pitot tube with an outer diameter of 3.9 mm and a tapered-nose Pitot tube with an outer diameter of 3.8 mm. For these two types of Pitot tubes, they saw that the calibration factor varied within $\pm 0.1\%$ or $\pm 0.2\%$ at speeds above 4 m/s; the maximum variation of the calibration factor is $\pm 0.5\%$ in the speed range of 1.8 m/s to 3.7 m/s, and the calibration factor varies from $\pm 1\%$ to $\pm 2\%$ at speeds lower than 1.2 m/s. On the other hand, Care and Fourneaux [10] found out that the pressure response depends on the design of the Pitot tube, and the resistance of the static pressure line mainly related to unexpected fluctuations of flow.

Chue [11] briefly outlined the generalized dimensions of several common Pitot tubes and discussed factors that cause measurement errors. However, no quantitative suggestion related to the calibration factor was given. Therefore, the ISO 3966 [12] and ASTM 3154 [13] suggested normative specifications regarding Pitot tube shapes, as presented in Table 1. In general, Pitot tubes have a head mounted on a stem. The total pressure hole and the static pressure holes are drilled into the

head of the Pitot tube. The axis of the head is parallel to the flow and perpendicular to the axis of its stem. The AMCA type of tube has a spherical head, as in Fig. 1(a). The surface finish is 0.8 μm , and the head is free from nicks and burrs [14]. The CETIAT type has a more complicated structure. This type has a nose with a conical shape. Static pressure holes are drilled and arranged on two parallel layers, as shown in Fig. 1 b. The NPL-type tube has a modified ellipsoidal nose. The profile definition of the ellipsoidal nose is described in Fig. 1 c. The junction between the stem and the body of the tube is curved or mitred.

ISO 3966 suggests working conditions and measurement methods of Pitot tubes, such as dimensional limitations, steady flow conditions, the Reynolds number, and the Mach number. The local velocity of the fluid also considers the relationship between the coefficient of the Pitot tube and other parameters, as equation (1):

$$V_p = \alpha(1 - \epsilon)\sqrt{\frac{2\Delta p}{\rho}} \quad (1)$$

The NPL Pitot tube coefficient depends on the distance from the plane of the static pressure holes to the stem. However, the commercial production of Pitot tubes is inhomogeneous because some countries still use their national standards. For instance, in Japan, Pitot tubes are manufactured following JIS B8330 [15], and the suggested value of α is equal to 1. On the other hand, some commercial manufacturers may use their internal standards, which may differ from the ISO standards.

Therefore, the main purpose of this study is to survey the geometry and performance of Pitot tubes fabricated with different manufacturers and determine the effects of the flow characteristics on their performance outcomes.

Table 1
Geometric parameters of pitot tubes recommended in international standards.

Parameter	D3154		ISO3966			B8330
d	AMCA 7.9	CETIAT 7.9	AMCA ≤ 15	CETIAT ≤ 15	NPL ≤ 15	Hemispherical tip N/A
d_i	4.0	N/A	$0.4d$	$0.125d$	N/A	$0.5d$
l_{ss}	$16d$	$16d$	$16d$	$14d$	$>8d$	$8d$
l_{sh}	$8d$	$8d$	$8d$	$6d$	$8d$	$6d$
α	N/A	N/A	1.00	1.00	1.0015	1
Re	N/A	N/A	≥ 200	≥ 200	≥ 200	N/A

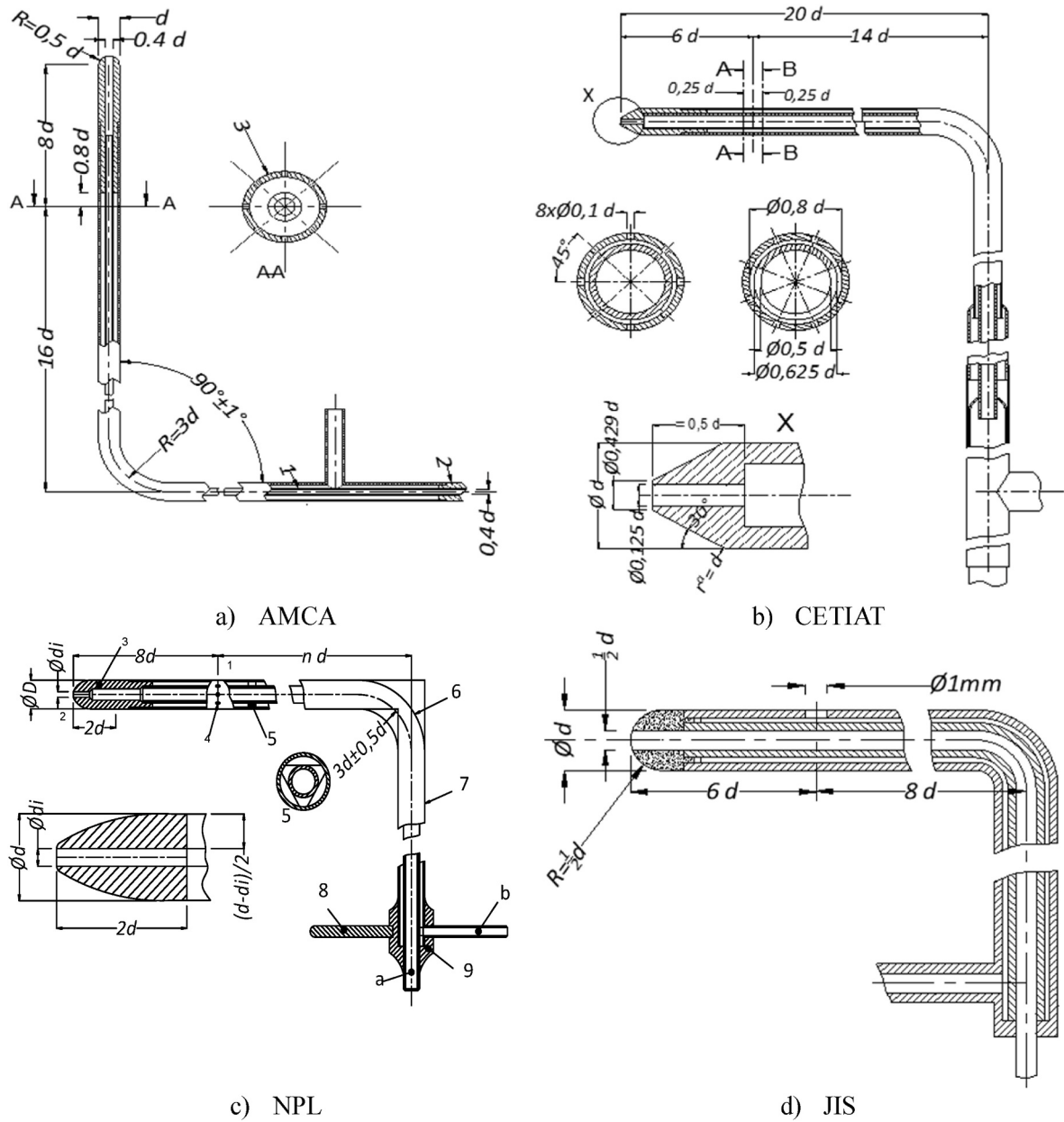


Fig. 1. Recommended designs of different types of Pitot tubes [10,12].

2. Experimental methods

2.1. Specifications of pitot tubes under test

To observe the effects of the geometry on the coefficients of Pitot tubes, 13 Pitot tubes were selected for testing. These consisted of four tubes of the NPL type, three tubes of the AMCA type, three tubes of the CETIAT type, and three tubes of the JIS type. A surface roughness tester measured the surface roughness levels of the 13 Pitot tubes with an accuracy of $\pm 2\% + 0.004 \mu\text{m}$. The specifications of these Pitot tubes are listed in Table 2. There are two interesting facts in Table 2. The first is that none of the AMCA tubes' l_{ss} values follows the ASTM or ISO 3966 guideline. The second is that no CETIAT type could be found in the market. Accordingly, three CETIAT-type tubes were procured via special order in Japan.

Table 2
Specifications of the pitot tubes.

Type	d	d_i	l_{sh}/d	l_{ss}/d
NPL	8.0	1.47	7.9	7.6
	6.0	1.38	8.0	8.4
	3.0	0.97	8.0	8.5
	2.4	0.84	7.8	8.6
AMCA	6.4	2.02	5.8	11.2
	4.7	1.87	6.1	11.6
	2.4	0.83	3.5	10.5
CETIAT	9.5	1.02	6.3	13.9
	6.5	0.75	6.3	14.0
	3.3	0.41	6.2	14.3
JIS	9.0	4.44	6.1	8.5
	6.0	2.95	6.1	8.4
	4.0	1.93	6.2	8.5

2.2. Experiments in a wind tunnel system

The effects of the flow characteristics on all of the Pitot tubes' coefficients were tested in NMIJ standard air speed systems. These systems consist of a medium wind tunnel (MWT) and a high air speed system (HASS). The MWT includes a Gottingen-type wind tunnel in which the test section area is $0.4 \text{ m} \times 0.4 \text{ m}$ and the operating range is from 1.3 m/s to 40 m/s , as shown in Fig. 2. The working standard for the wind tunnel is an ultrasonic anemometer mounted on the wall of the test section. An LDA system was calibrated with an ultrasonic anemometer, and the LDA system was calibrated against a rotating disc [16]. The expanded uncertainty values of the MWT are $(0.297 + 0.27/v^2 - 0.77v) \%$ from 1.3 m/s to 27.5 m/s and $(-0.0001185v^3 + 0.01157v^2 - 0.3677v + 4.124) \%$ from 27.5 m/s to 40 m/s [17].

The HASS in Fig. 3 is an open-jet type in which the test section diameter is 100 mm , and the working range is from 30 m/s to 90 m/s . The maximum turbulent intensity in the test section is below 0.3% . The working standard for the wind tunnel is a jet nozzle which is calibrated by a gas flow standard system [16,18]. The expanded uncertainty value of the HASS is 0.63% with $k = 2$.

2.3. Method of measurement and analysis

To determine the coefficient curve, Pitot tubes were placed in a holder and aligned in the flow directions of the MWT and HASS. The device used for checking the alignment of the testing Pitot tubes includes a precise ruler attached perpendicular to a block level. The body of the Pitot tube is perpendicular to the flow direction as it is adjusted parallelly to the vertices of the ruler. Then, the stem of the Pitot tube is adjusted parallelly to the edge of the ruler. Two adjustment steps ensure the head of the Pitot tube will keep aligned to the flow direction within $\pm 0.1^\circ$. The air speed for the testing measurements was varied from 2 m/s to 90 m/s . For the velocities of **(2, 3, 5, 7, 10, 15, 20, 25, 30, 35, and 40)** m/s , the coefficients of the Pitot tubes were determined on the MWT. For the velocities of $(30, 40, 50, 60, 70, 80, \text{ and } 90) \text{ m/s}$, the coefficients of the Pitot tubes were determined on the HASS. Here, 30 m/s and 40 m/s

are the overlapping points; thus, these points were selected to check the consistency between MWT and HASS. This consistency was ensured because all values of the normalized error exceeded 1 . The method for determining the normalized deviation is presented in Appendix A3. At each velocity, the test was repeated five times, and the value of each time was averaged from 60 data recorded within 1 min .

Based on Bernoulli's theory of the MWT system, the velocity of the Pitot tube was equal to the velocity of a reference, V_s in equation (1). Then, α is calculated using equation (2):

$$\alpha = \frac{V_s}{(1 - \epsilon) \sqrt{\frac{\Delta p}{\rho}}} \quad (2)$$

In addition, following the research of Iwai et al. [18], α of the Pitot tubes on the HASS system is calculated using equation (3):

$$\alpha = C_{\text{HASS}} \sqrt{\frac{\Delta p_{\text{HASS}}}{\Delta p}} \quad (3)$$

To estimate how the flow characteristics affect the Pitot tubes, the tests were conducted over a range of Reynolds numbers for which the Reynolds number was defined according to the length scale of both the outer head diameter and the inner head diameter of the tubes as equation (4):

$$Re_d = \frac{\rho V_p d}{\mu} \quad \text{or} \quad Re_{d_i} = \frac{\rho V_p d_i}{\mu} \quad (4)$$

3. Results and discussions

3.1. Effects of geometry on the pitot tube coefficient

Through the setup and method described in sections 2.2 and 2.3, the experimental data for the four types of Pitot tubes were calibrated, and the coefficients of the Pitot tubes were presented against the velocity for an analysis.

For the NPL Pitot tubes group, the data in Fig. 4 show that the

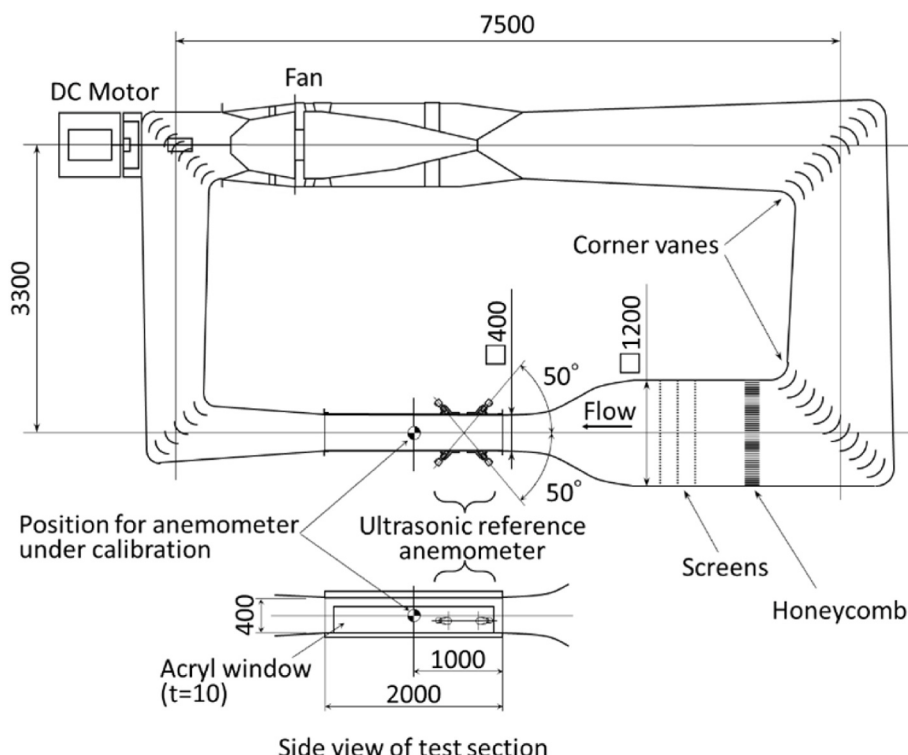


Fig. 2. Medium wind tunnel.

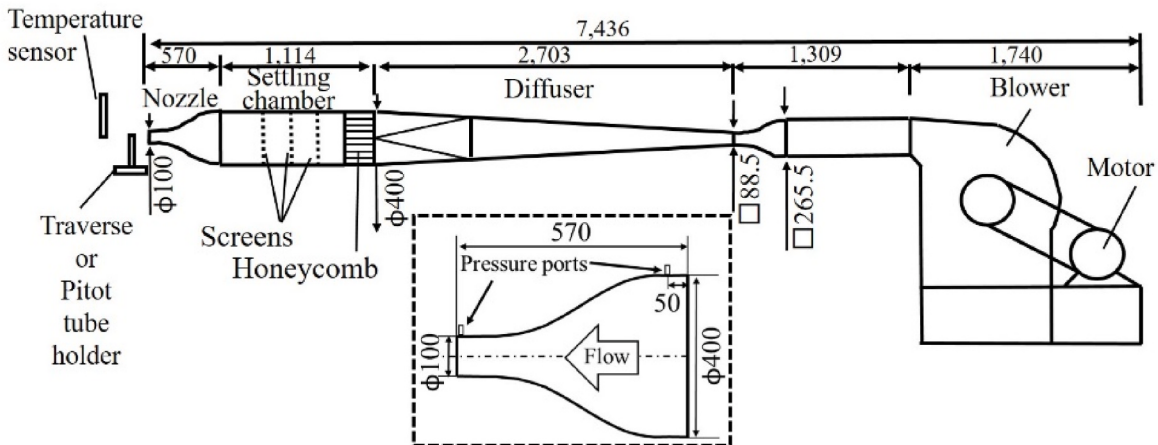


Fig. 3. High air speed standard system.

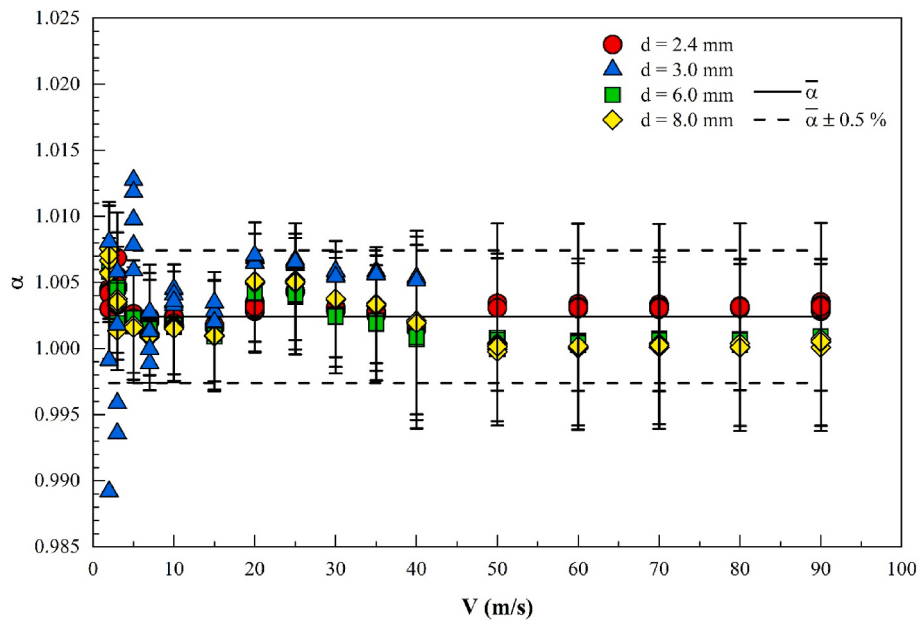


Fig. 4. Coefficients of NPL Pitot tubes.

coefficients scatter at velocities lower than 5 m/s. In this region of velocity, the scatter of the coefficients is 0.6%. This result is consistent with the investigation of Ower and Johansen [19]. Moreover, the coefficients are larger by 0.3% compared to the reference value of 1.0015 suggested in ISO 3966. Meanwhile, at velocities greater than 5 m/s, the coefficients become more stable, and the scattering is $\pm 0.4\%$. The expanded uncertainty in these cases fluctuates slightly in the range of 0.0041–0.0070. In general, the average coefficient of the NPL Pitot group is 1.0024. This value differs by 0.1% from the reference value. The components contribute to the uncertainty of α , and the uncertainty estimation results are presented in Appendix A1 and Appendix A2. In this group, the NPL tube with $d = 3.0$ mm has the greatest fluctuation compared to the others at a low velocity. This scattering is quantified as 3.8%. The expanded uncertainty increases to 0.0392 and 0.0292 at 2 m/s and 3 m/s, respectively. This result will be discussed in section 3.2.

Similar to the NPL Pitot tube, AMCA Pitot tubes' coefficients are scattered at velocities lower than 5 m/s, as shown in Fig. 5. However, the scattering level is 1.8%, which is larger than that of the NPL tubes. At 2 m/s and 3 m/s, the most significant expanded uncertainty values of the AMCA Pitot tubes are correspondingly 0.0144 and 0.0083. Furthermore,

the coefficient value is relatively stable at velocities exceeding 5 m/s. Fig. 5 shows that the Pitot coefficients are mostly stable in the HASS system. These experimental results only differ by less than 0.15% from the reference value recommended in ISO 3966. Generally, the average coefficient of the AMCA Pitot tube group is 1.0010 and differs by 0.1% from the reference value. On the other hand, as mentioned in section 2.1, all AMCA tubes tested in this study violate the shape guidelines recommended in ISO 3966. In detail, all parameters of l_{sh} and l_{ss} are smaller than 8 and 16, respectively, as shown in Table 2. However, the performance capabilities of AMCA Pitot tubes remain adequate. Therefore, the ISO standard may require some revisions in the guideline for AMCA Pitot tubes.

Fig. 6 shows that the coefficient curves of the CETIAT Pitot tubes are fairly similar to those of the NPL type. Their expanded uncertainties are also in the range of 0.0041–0.0071. The maximum magnitude of tolerance compared to their reference coefficient is 0.65% when the velocities exceed 5 m/s in the MWT system. This is also true at all velocities in the HASS system. In the CETIAT group, the CETIAT tube with $d = 3.3$ mm shows significant scattering at velocities lower than 10 m/s. Fig. 7 shows that the α value has a standard deviation of 0.18 at 2 m/s.

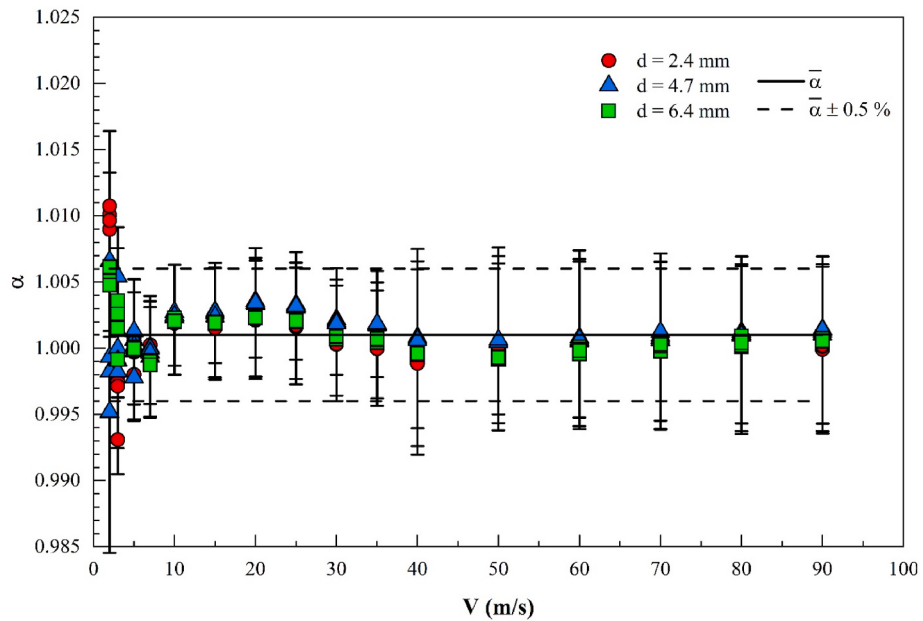


Fig. 5. Coefficient curve of AMCA Pitot tubes.

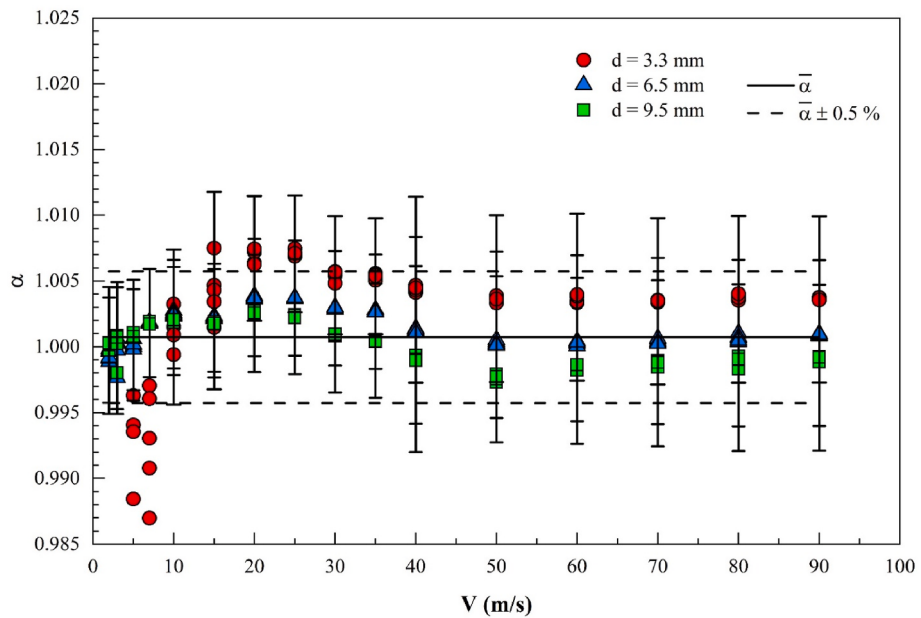


Fig. 6. Coefficient curve of CETIAT Pitot tubes.

This value exceeds by many times the values of the other samples at the same velocity. Thus, this result is analyzed and discussed in detail in section 3.2.

For the JIS Pitot tubes, the data in Fig. 8 show that nearly all coefficients are larger than 1 at the testing air speeds and that their standard deviation is 0.3%. Therefore, their average value is 1.0054 and is slightly larger by 0.5% than the reference value of 1 recommended in JIS B8330. However, the JIS Pitot tubes' performance is stable at low air speeds, and their expanded uncertainties range from 0.0032 to 0.0066.

This outcome is similar at high air speeds, but the corresponding expanded uncertainties remain stable at 0.0064. On the other hand, the starting point of the distance from the total pressure hole to the static holes was not clearly defined in JIS B8330 [15]. This occurs because the head tip point in Fig. 1(d) starts from the left end of the head, but that point disappears after the total pressure hole is made by drilling or any

others.

3.2. Effect of the pressure response

As mentioned in section 3.1, NPL Pitot tube 3.0 has anomalous scattering at 2 m/s and 3 m/s compared to the others. The surface of Pitot tube NPL 3.0 was carefully checked with a magnifier. This test found burrs and paraffin remaining in the total pressure holes and the static holes, as shown in Fig. 9. In addition, its surface underwent a surface treatment with sandblasting. The Pitot tube's surface roughness is repeatedly measured five times on two faces of the Pitot tube and averaged. The measured R_a values of the Pitot tubes are listed in Table 3. To observe the effect of roughness on the performance of NPL Pitot tubes, the relative roughness R_a/d is used for observing how the coefficients of NPL Pitot tubes change. Fig. 10 presents that NPL Pitot tube

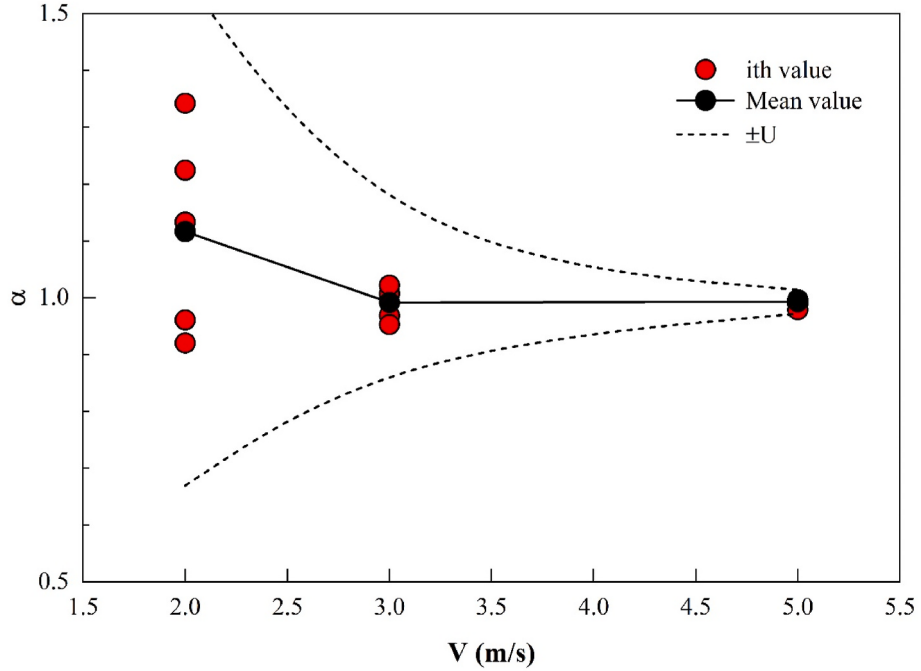


Fig. 7. Coefficient values of CETIAT 3.3 Pitot tubes.

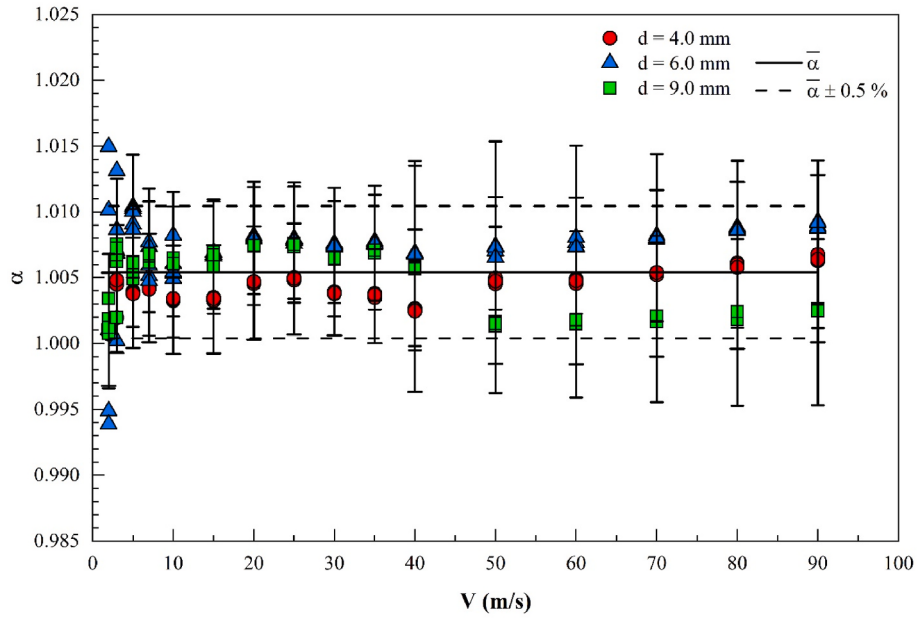


Fig. 8. Coefficient curve of JIS Pitot tubes.

3.0 with the highest R_a/d has a considerable variation in its coefficient than others at velocities smaller than 5 m/s. On the contrary, NPL Pitot tube 8.0 has a value of R_a/d less than NPL Pitot tube 3.0 ten times, and its coefficients show the maximum deviation of 0.4% at testing velocities smaller than 5 m/s. Theoretically, since the relative roughness increases, recirculation and flow separation arise in the flow passing over the roughness feature. Then, the dynamic pressure will become unstable. Therefore, the dispersion of α of the NPL Pitot tube 3.0 at low testing velocities may relate to the high relative roughness. However, as testing velocities increase more than 5 m/s, the dispersion of α attenuates. This result agrees with the research of Kandlikar and Schmitt [20]. They found that since roughness increases at the surface, a transition occurs in the Reynolds number range of 350 and 800.

To verify this experimentally, an NPL Pitot tube's head surface with $d = 3.0$ mm was made smooth by an oil coating and then recalibrated. The fluctuations of the dynamic pressure values improved with this surface treatment, as shown in Fig. 11. Moreover, the variation of α is 4.5% after removing the burrs and paraffin. In the initial condition, this variation is 6.5%. Furthermore, there was a significant improvement when applying the oil coating. The variation was reduced to 0.7% and 2.9% at 2 m/s and less than 2 m/s, respectively. Hence, Fig. 12 shows that the expanded uncertainty of α at 2 m/s and 3 m/s was reduced to 0.0207. However, at velocities exceeding 5 m/s, the roughness does not affect the Pitot tube coefficients, as their values do not show any changes. Similar to NPL Pitot tube 3.0, the α value for CETIAT 3.3 mm is strongly dispersed at 2 m/s and 3 m/s. The CETIAT tube has more

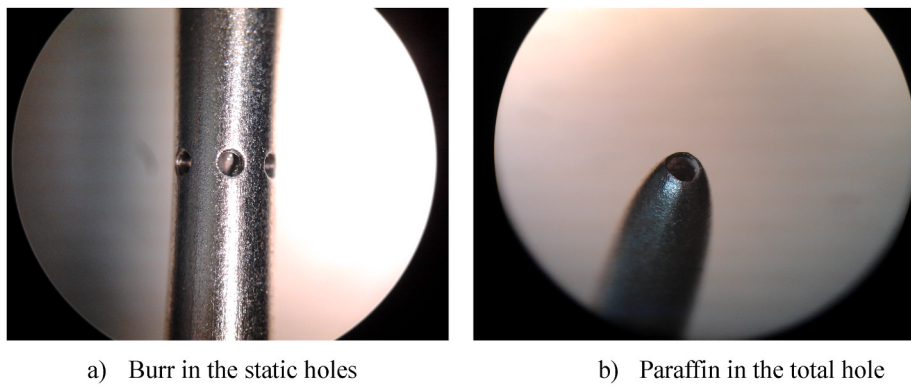
Fig. 9. Surface and hole conditions of a NPL Pitot tube with $d = 3.0$ mm.

Table 3
Surface roughness values of the pitot tubes.

Type	d	R_a	R_a/d
NPL	8.0	0.15	0.00002
	6.0	0.82	0.00014
	3.0	0.59	0.0002
	2.4	0.14	0.00006

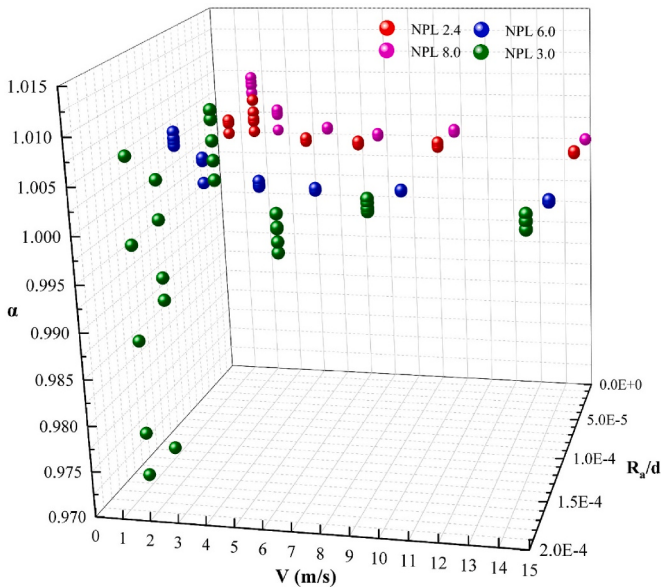


Fig. 10. Effect of roughness on the coefficients of NPL Pitot tubes.

complexity in its design than other types of Pitot tubes. Its static holes are arranged in double rows, as shown in Fig. 1(b). Consequently, for CETIAT 3.3 mm, the reason for its problem comes from a mistake in the design. The gap between the two concentric total pressure and static pressure holes is too narrow at only 0.1 mm. This causes a different response between the total pressure and the static pressure. The total pressure needs only 40 s to stabilize. However, the static pressure needs almost 100 s to become stable. As a result, this delay time makes the fluctuation of the coefficient when the velocity changes. Simultaneously, it also explains that the other CETIAT Pitot required 1 min to stabilize their differential pressure. In contrast, a time of 2 min was required for CETIAT 3.3 mm, as Fig. 13. Primarily, this influence strongly imposes on the low velocities. At velocities smaller than 5 m/s, the Pitot coefficient has a big scattering and results in considerable standard deviation and uncertainty, as shown in Fig. 7. Due to the

structure complexity, the CETIAT tube has a high cost and is prone to errors during the manufacturing process. To simplify the structure, a CETIAT type Pitot tube with one row of static pressure holes should be tested in future work. In this experiment, the new design of the CETIAT 3.3 mm with a 0.3 mm gap between the two concentric tubes gives satisfactory results. It resolves the delay time in the pressure responses that the old design has. The coefficient and scattering were considerably reduced at the low air speed. At velocities smaller than 5 m/s, the coefficient's standard deviation reduces up to 18 times, from 0.18 down to 0.01. Furthermore, at 2 m/s, the average value of coefficient that differs from the reference value recommended in ISO [12] is 2.1% instead of 11% in the old design shown in Figs. 7 and 14, respectively. Fig. 14 also shows better consistency in the coefficient value and the uncertainty between the new design and other CETIAT tubes.

3.3. Effect of the Reynolds number

Related to the effect of the flow characteristics on the Pitot tubes' performance, the variation of the Pitot tubes' coefficient values was observed when the Reynolds numbers ranged from 40 to 1×10^5 . According to ISO 3966 [12], the Reynolds number is determined based on a Pitot tube's head outer diameter, Re_d . However, Mikhailova and Repik [21] recommended that for all Pitot tubes with $\beta < 0.6$, the length scale of the Reynolds number is the head inner diameter of the Pitot tube, Re_{d_i} . In detail, Mikhailova and Repik proved that when β has a small value, the tubes are strongly affected by the viscosity, but when $\beta > 0.6$, they suggested Re based on the tube's outer diameter. Due to the difference between the ISO standard and the values in earlier research, this study observes the flow characteristic effect based on both length scales, i.e., the head inner diameter and the outer diameter of the tubes. The experimental results are plotted over Reynolds numbers ranging from 40 to 1×10^5 , as shown in Fig. 15 for Re_{d_i} or Re_d . Boetcher and Sparrow [6] suggested that the Bernoulli theory should not be used when $Re < 45$. All Pitot tubes in the present experiments theoretically comply with Bernoulli's interpretation. In the range of $40 < Re_{d_i} < 10^2$, only CETIAT 3.3 mm and CETIAT 6.5 mm apply, and the α value for CETIAT 3.3 mm differs from the corresponding average value by 2.1%. This result is consistent with the 2% error of α presented in Boetcher and Sparrow [4]. In the range of $10^2 < Re_{d_i} < 10^3$, all other Pitot tubes show stable α values with variations from the reference value of 0.1%–0.5%, but NPL 3.0 has a difference of up to 2.5%.

On the other hand, if using the variable Re_d , the majority of the Pitot coefficients are less than 1, and those are strongly dispersed when $Re_d < 700$. These results disagree with the suggestion of ISO 3966 [12] as the Reynolds number exceeds 200. However, when the Reynolds number is within the range of 10^3 to 10^5 , the α values become stable and form linear trends on the scale of Re_{d_i} as well as Re_d . Comparing to the Pitot tubes' reference values, their maximum deviations are 0.1% for the AMCA, 0.4% for the CETIAT, 0.3% for the NPL, and 0.9% for the JIS

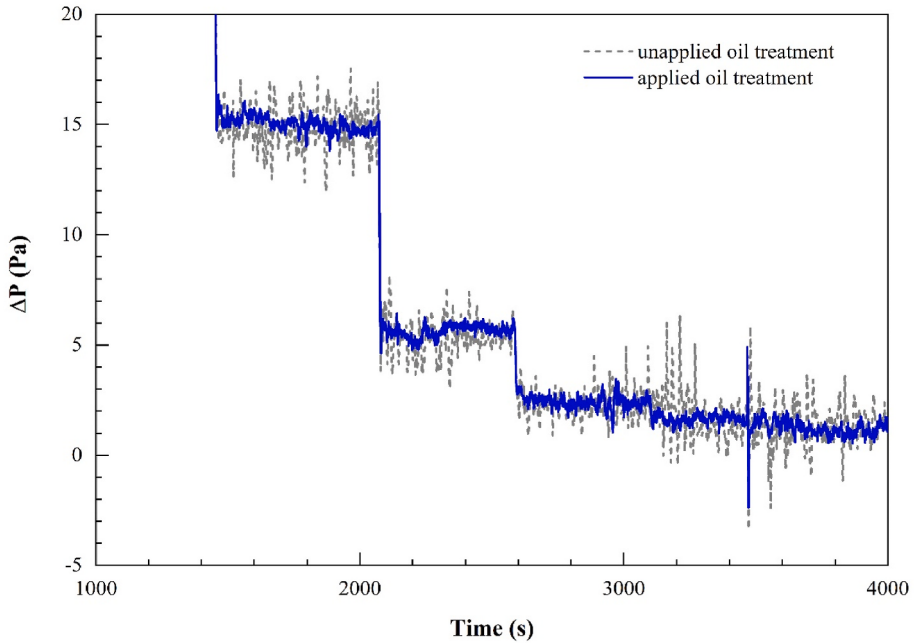


Fig. 11. Effect of the surface roughness on the dynamic pressure.

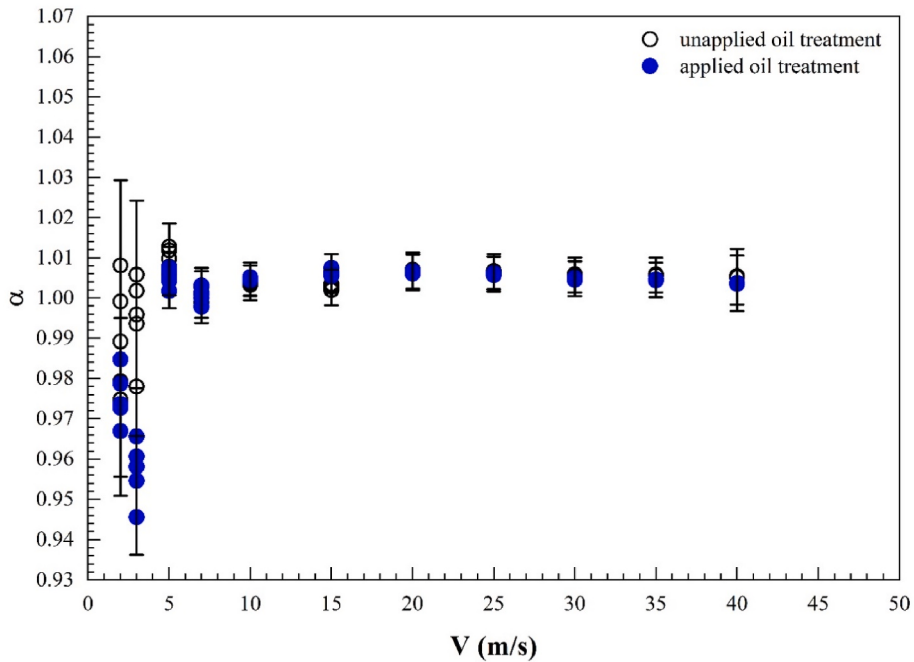


Fig. 12. Performance of the NPL 3.0 Pitot tube before and after a surface treatment.

Pitot tubes.

In summary, the scale of Re_{d_i} shows the flow characteristics on the coefficient curve of Pitot tubes better than the scale of Re_d . However, in general, the two trends are nearly identical. This result complies with the conclusion of Spelley et al. [7] that Pitot tubes with a thick wall can use the inner head diameter as the length scale parameter.

4. Conclusions

This study investigated the performance capabilities of four different types of static tubes in the standards. The conclusions are as follows:

1. In ISO, the verification of working conditions for a static Pitot is in $Re_{d_i} > 200$. However, generally the coefficient curve of Pitot tubes based on the flow characteristics of both of the length scales d_i and d are nearly identical. Therefore, the length scale d can be used in practice as a convenience. The performance of Pitot tubes is stable at Reynolds numbers larger than 600, with the outer head diameter as the length scale parameter. As $Re_d < 700$, all static Pitot tubes' coefficient values fluctuate considerably and contain errors compared to the values recommended in the ISO and JIS standards.
2. At velocities from 5 m/s to 90 m/s, the AMCA type of Pitot tube has coefficients that are more stable and homologous than those of other types despite having shape dimensions that differ from the

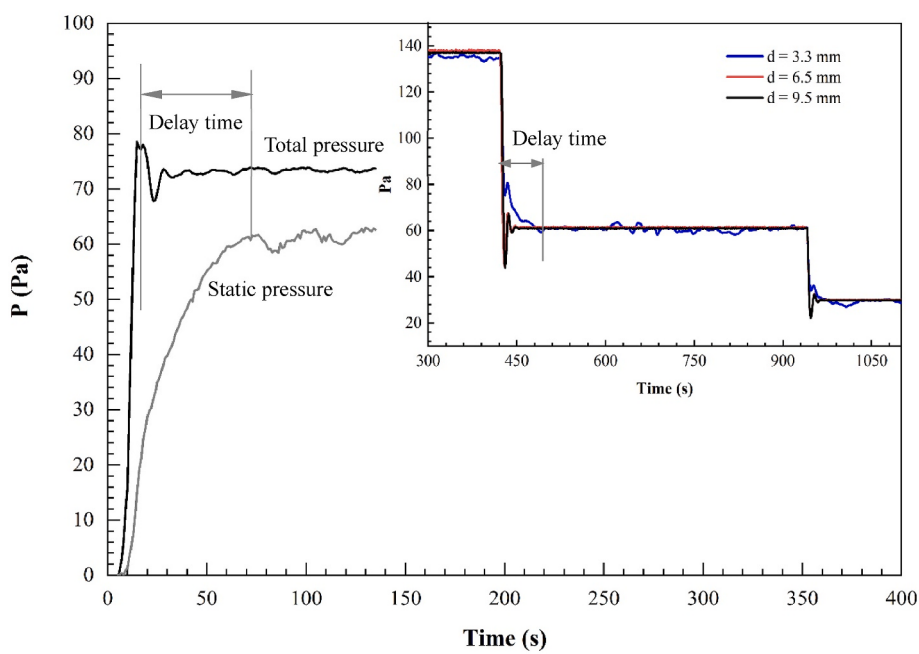


Fig. 13. Pressure response of CETIAT Pitot tubes.

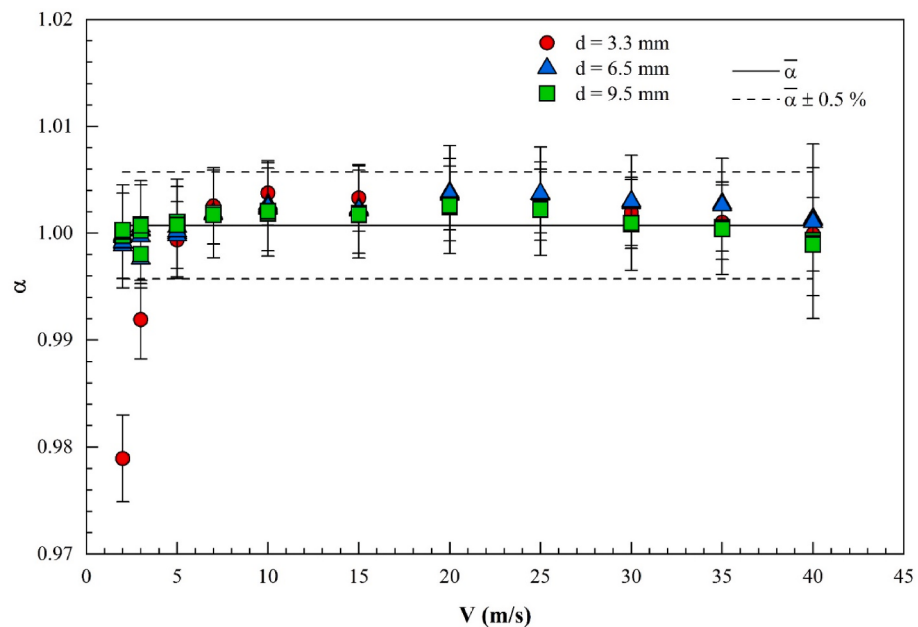


Fig. 14. Performance of the CETIAT new design.

recommendation in ISO 3699. Moreover, as the velocity increases to 90 m/s ($Ma > 0.25$, Ma : Mach number), all Pitot tubes' coefficient curves remain linear.

3. All JIS Pitot tubes have coefficient values larger than the reference value of 1 specified in the JIS standard.
4. The surface roughness affects Pitot tube performance outcomes; therefore, this effect must be quantified in future work. Moreover, simplification of the CETIAT Pitot tube initially gives good results. Accordingly, additional and more detailed research should be conducted to develop this type as a commercial instrument. This can be a future research topic.

Authorship contributions

Yong Moon Choi: Conceptualization, Design of methodology, Creation of models and experiments, Analysis and interpretation of data, Validation, reproducibility of results, Revising the manuscript critically for important intellectual content, Visualization, Approval of the version of the manuscript to be published. **Yoshiya Terao:** Design of methodology, Validation, reproducibility of results, Revising the manuscript critically for important intellectual content, Approval of the version of the manuscript to be published. **Noboru Kurihara:** Creation of models and experiments. **Aya Iwai:** Creation of models and experiments, Validation, reproducibility of results. **Tatsuya Funaki:** Creation of models and experiments. **Woong Kang:** Analysis and interpretation of data, Revising the manuscript critically for important intellectual content.

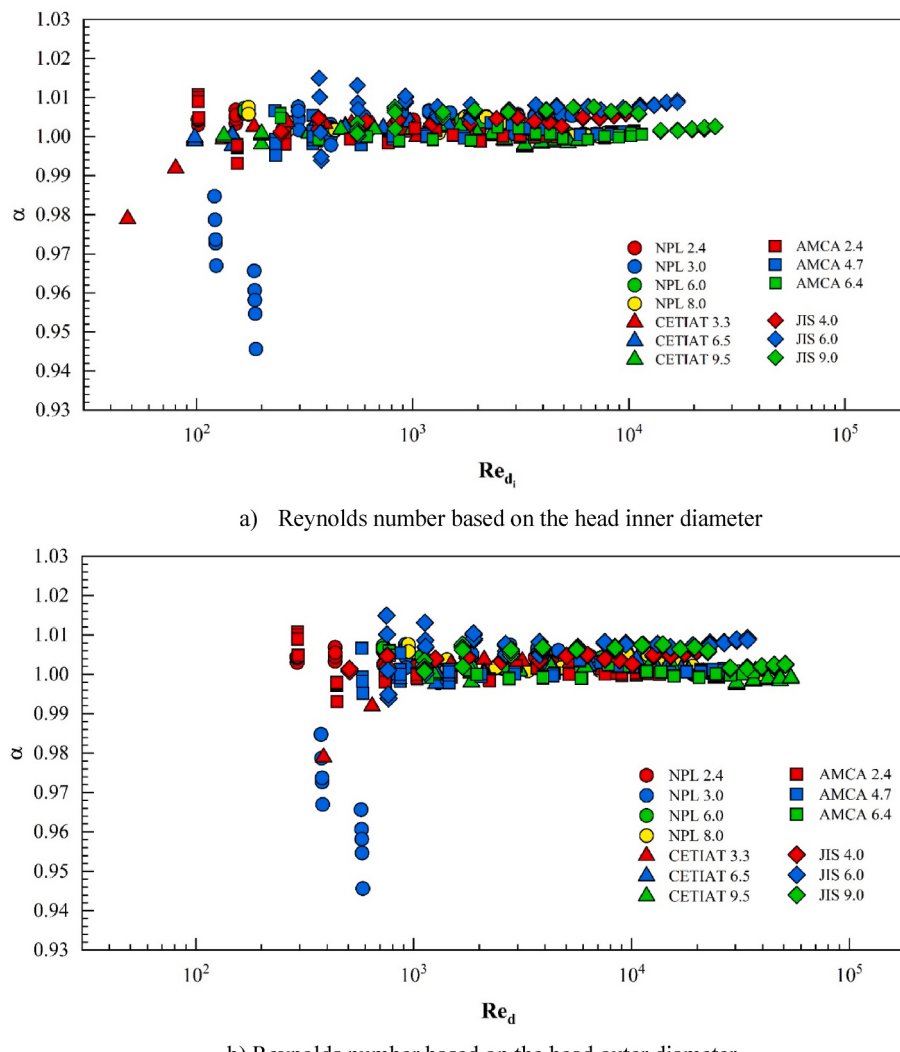


Fig. 15. Relationship between the Reynolds number and all Pitot coefficients.

Nguyen Doan Trang: Analysis and interpretation of data, Drafting the manuscript, Revising the manuscript critically for important intellectual content, Visualization.

Declaration of competing interest

The authors declare that they have no known competing financial interests or personal relationships that could have appeared to influence the work reported in this paper.

Appendix. Uncertainty analysis

A.1. Estimating the uncertainty of Pitot tubes on the MWT system

As described in section 2.3, the coefficients of Pitot tubes on the MWT system are calculated as shown as equation (2)

$$\alpha = \frac{V_s}{(1 - \varepsilon) \sqrt{\frac{\Delta p}{\rho}}} \quad (2)$$

Following ISO 3966, $(1-\varepsilon)$ is determined as equation A.1:

$$1 - \varepsilon = \left[1 - \frac{1}{2\gamma} \frac{\Delta p}{P} + \frac{\gamma - 1}{6\gamma^2} \left(\frac{\Delta p}{P} \right)^2 \right]^{\frac{1}{2}} \quad (A.1)$$

Referring to the brief equation of CIPM 81 [22], the density of air is calculated via equation A.2

$$\rho = \frac{0.34844P + \varphi(-0.00252T + 0.020582)}{T + 273.15} \quad (A.2)$$

Assuming that the input parameters of the mathematic models were mutually independent, according to the ISO guide [23], equation 2 and A.2 can

be expressed as the following uncertainty propagation by means of a Taylor series approximation in [equation A.3](#) and [A.4](#).

$$u^2(\alpha) = c_{V_s}^2 u^2(V_s) + c_{(1-\varepsilon)}^2 u^2(1 - \varepsilon) + c_{\Delta p}^2 u^2(\Delta p) + c_\rho^2 u^2(\rho) \quad (\text{A.3})$$

$$u^2(\rho) = c_p^2 u^2(P) + c_{(T)}^2 u^2(T) + c_\varphi^2 u^2(\varphi) \quad (\text{A.4})$$

Here, c_{V_s} , $c_{(1-\varepsilon)}$, $c_{\Delta p}$, c_p , c_T , c_φ are the sensitivity coefficients of V_s , $(1 - \varepsilon)$, Δp , P , T , and φ .

Because the air speed varies at 2, 3, 5, 7, 10, 15, 20, 25, 30, 35 and 40 m/s on the MWT system, $u(V_s)$ can represent the uncertainty of the MWT system at the approximate air speed. The standard uncertainty of the static pressure, temperature, and humidity is the standard uncertainty of this measurement instrument.

On the other hand, for equation (5), in order to reduce the differential calculation, the uncertainty of a compressibility correction factor is estimated according to the numerical analysis in ISO 5168. By applying a small change to Δp , γ , and P , the effect on the compressibility correction will be observed. Here, the standard uncertainty of Δp , γ , and P is selected as the small change corresponding change in Δp , γ , and P . The sensitivity coefficients are calculated against the fraction of an increment of the compressibility correction factor and the small change in the input.

Finally, in order to determine $u_A(\alpha)$, the measurements were done repeatedly, with the average value then determined via [equation A.5](#) and [A.6](#).

$$\bar{\alpha} = \frac{1}{n} \sum_{i=1}^n \alpha_i \quad (\text{A.5})$$

$$u_A^2(\alpha) = \frac{1}{n-1} \sum_{i=1}^n (\alpha_i - \bar{\alpha})^2 \quad (\text{A.6})$$

By combining equations A.3 and A.6, the combined uncertainty of the measurement of α is expressed as shown in [equation A.7](#):

$$u_c(\alpha) = \sqrt{u_A^2(\alpha) + u^2(\alpha)} \quad (\text{A.7})$$

From equation A.7, the expanded uncertainty of the measurement is a multiple of the combined uncertainty and the coverage factor ($k = 2$) as [equation A.8](#):

$$U = 2 \times u_c(\alpha) \quad (\text{A.8})$$

As an example, the uncertainty AMCA Pitot tube 2.4 at 2 m/s is presented in [Table A.1](#).

A.2. Estimating the uncertainty of a Pitot tube on the HASS system

As mentioned in section 2.2, following the research of Iwai et al. [18], the α values of Pitot tubes on the HASS system were calculated using [equation 3](#):

$$\alpha = C_{\text{HASS}} \sqrt{\frac{\Delta p_{\text{HASS}}}{\Delta p}} \quad (3)$$

Simultaneously, the uncertainty of α on the HASS system was estimated in detail in Iwai et al. [18]. The maximum relative combined uncertainty derived from the calibration of the Pitot tube, $u(\alpha)$, equals 0.32×10^{-2} at an air speed of 40 m/s. Using this value and equations A.5 to equation A.7, the expanded uncertainty of the measurement of α is expressed as [equation A.8](#).

For example, the uncertainty of AMCA Pitot tube 2.4 mm at 90 m/s is presented in [Table A.2](#).

A.3 Estimating the consistency between MWT and HASS

As mentioned in section 2.3, the airspeeds of 30 m/s and 40 m/s are the points at which the coefficients of the Pitot tubes were determined in both the MWT and HASS systems. Therefore, based on these coefficients collected from the MWT and HASS systems, the reference value (RV) between the data measured in the MWT and HASS systems followed Cox [24] as [equation A.9](#):

$$RV = \frac{\frac{\alpha_{\text{MWT}}}{u^2(\alpha_{\text{MWT}})} + \frac{\alpha_{\text{HASS}}}{u^2(\alpha_{\text{HASS}})}}{\frac{1}{u^2(\alpha_{\text{MWT}})} + \frac{1}{u^2(\alpha_{\text{HASS}})}} \quad (\text{A.9})$$

In this equation, α_{MWT} and α_{HASS} are the coefficient of each Pitot tube determined in the MWT and HASS systems; u_{MWT} and u_{HASS} are the standard uncertainty values of each Pitot tube's coefficient, and RV is the weighted mean of each Pitot tube's coefficient.

The standard uncertainty associated with the RV value is calculated as [equation A.10](#):

$$u(RV) = \frac{1}{\frac{1}{u^2(\alpha_{\text{MWT}})} + \frac{1}{u^2(\alpha_{\text{HASS}})}} \quad (\text{A.10})$$

Then, all Pitot tube's coefficients are overall consistent if their chi-squared test satisfies [equation A.11](#) and [A.12](#).

$$\chi_{\text{obs}}^2 = \frac{(\alpha_{\text{MWT}} - RV)^2}{u^2(\alpha_{\text{MWT}})} + \frac{(\alpha_{\text{HASS}} - RV)^2}{u^2(\alpha_{\text{HASS}})} \quad (\text{A.11})$$

$$\Pr\{\chi^2(\nu) > \chi_{\text{obs}}^2\} > 0.05 \quad (\text{A.12})$$

When the consistency checks pass, the degree of equivalence of each Pitot tube's coefficient displays some deviation from the RV at 40 m/s, and it has expanded uncertainty at the 95% level of confidence as equation A.13 and A.14:

$$\text{DoE} = \alpha_i - \text{RV} \quad (\text{A.13})$$

$$U(\text{DoE}) = 2u(\text{DoE}) \quad (\text{A.14})$$

where $u(\text{DoE})$ is given by $u^2(\text{DoE}) = u^2(\alpha) - u^2(\text{RV})$.

Moreover, the consistency of the Pitot tube's coefficient measured in the MWT and HASS systems is indicated by the normalized error, E_n as equation A.15. When $|E_n| < 1$, it is assumed to show this consistency.

$$E_n = \frac{\text{DoE}}{U(\text{DoE})} \quad (\text{A.15})$$

The normalized errors of all Pitot tubes at 30 m/s and 40 m/s are listed in Table A.3 and Table A.4, respectively. These values are all smaller than 1 at 30 m/s and 40 m/s. As a result, all experimental data obtained in the MWT and HASS systems are consistent.

Table A.1
Uncertainty Budget of AMCA Pitot tube 2.4 mm at 2 m/s

Source of uncertainty	Standard uncertainty	Sensitivity coefficient
Compressibility correction factor	2.87×10^{-7}	-9.8×10^{-1}
Static pressure in MWT	4.766 Pa	3.6×10^{-8}
Dynamic pressure	0.016 Pa	8.9×10^{-6}
Ratio of specific heat capacity	0.0035	5.2×10^{-5}
The density of air	0.0003 kg/m ³	0.42
Humidity in MWT	0.75 %RH	-1.5×10^{-4}
Temperature in MWT	0.065 °C	-3.96×10^{-3}
Static pressure in MWT	0.047 hPa	1.16×10^{-3}
MWT system	0.004 m/s	0.49
Dynamic pressure	0.0104 Pa	-0.21
Resolution of differential pressure gauge	0.0003 Pa	-0.21
Differential pressure gauge	0.0018 Pa	-0.21
Standard deviation of the dynamic pressure value	0.01 Pa	-0.21
Standard uncertainty of α	0.0023	1
Combined uncertainty of α	0.0038	
Coverage factor	2	
Expanded uncertainty, U	0.0076	

Table A.2
Uncertainty Budget of AMCA Pitot tube 2.4 at 90 m/s

Source of uncertainty	Standard uncertainty	Sensitivity coefficient
Type B uncertainty of α	0.032	1
Standard uncertainty of α	0.00016	1
Combined uncertainty of α	0.0032	
Coverage factor	2	
Expanded uncertainty, U	0.0063	

Table A.3
Results of the Consistency Test for the Pitot Tubes at 30 m/s.

Pitot tube	RV	$U(\text{RV})$	χ_{obs}^2	$n-1$	$\Pr\{\chi^2(\nu) > \chi_{\text{obs}}^2\} > 0.05$	E_n	Result
NPL 8.0	1.0019	0.0034	0.010	4	1	0.050	Pass
NPL 6.0	1.0009	0.0034	0.000	4	1	0.005	Pass
NPL 2.4	1.0016	0.0034	0.004	4	1	0.031	Pass
CETIAT 9.5	0.9990	0.0035	0.010	4	1	0.049	Pass
CETIAT 6.0	1.0012	0.0035	0.002	4	1	0.020	Pass
CETIAT 3.3	1.0043	0.0035	0.001	4	1	0.016	Pass
AMCA 6.4	0.9996	0.0034	0.002	4	1	0.020	Pass
AMCA 4.7	1.0007	0.0034	0.000	4	1	0.007	Pass
AMCA 2.4	0.9991	0.0033	0.010	4	1	0.049	Pass
JIS 9.0	1.0058	0.0269	0.027	4	1	0.082	Pass
JIS 6.0	1.0068	0.0035		4	1	0.001	Pass
JIS 4.0	1.0035	0.0022	0.225	4	1	0.237	Pass

Table A.4

Results of the Consistency Test for the Pitot Tubes at 40 m/s

Pitot tube	RV	$U(RV)$	χ^2_{obs}	$n-1$	$\Pr\{\chi^2(\nu) > \chi^2_{\text{obs}}\} > 0.05$	E_n	Result
NPL 8.0	1.0037	0.0022	0.006	4	1	0.038	Pass
NPL 6.0	1.0025	0.0022	0.000	4	1	0.006	Pass
NPL 2.4	1.0030	0.0022	0.001	4	1	0.013	Pass
CETIAT 9.5	1.0010	0.0022	0.017	4	1	0.065	Pass
CETIAT 6.0	1.0029	0.0022	0.002	4	1	0.022	Pass
CETIAT 3.3	1.0054	0.0022	0.000	4	1	0.008	Pass
AMCA 6.4	1.0087	0.0022	0.008	4	1	0.045	Pass
AMCA 4.7	1.0020	0.0020	0.001	4	1	0.018	Pass
AMCA 2.4	1.0004	0.0022	0.000	4	1	0.001	Pass
JIS 9.0	1.0064	0.0022	0.009	4	1	0.048	Pass
JIS 6.0	1.0075	0.0022	0.000	4	1	0.001	Pass
JIS 4.0	1.0041	0.0014	0.156	4	1	0.197	Pass

References

- [1] M. Pitot, Description d'une Machine pour mesurer la vitesse des Eaux courantes, & le sillage des Vaisseaux, Hist, l'Academie R. Des Sci. (1732) 363–376.
- [2] H. Darcy, Note relative à quelques modifications à introduire dans le tube de Pitot, Ann. Des Ponts Chaussees. 1 (1958) 351–359.
- [3] G. Brown, Henry Darcy and pitot tube, in: Third Natl. Congr. Civ. Eng. Hist. Herit., 2001.
- [4] M. Barker, On the use of very small pitot-tubes for measuring wind velocity, Proc. R. Soc. A. 101 (1922) 435–445.
- [5] F.A. Macmillan, Viscous effects on pitot tubes at low speeds, J. R. Aeronaut. Soc. 58 (1954) 570.
- [6] S.K.S. Boetcher, E.M. Sparow, Limitations for the standard Bernoulli equation method for evaluating Pitot/impact tube data, Int. J. Heat Mass Tran. 50 (2007).
- [7] R.B. Spelay, K.F. Adane, R.S. Sanders, J.S. Robert, R.G. Gillies, The effect of low Reynolds number flows on pitot tube measurements, Flow Meas. Instrum. 45 (2015) 247–254.
- [8] E. Ower, F.C. Johansen, The Design of Pitot Static Tubes, R. M., 1925.
- [9] E. Ower, R.C. Pankhurst, The Measurement of Air Flow, Pergamon Press, 1977.
- [10] I. Care, R. Fourneaux, Investigation of the pressure response of different Pitot tubes, Flow Meas. Instrum. 72 (2020) 714.
- [11] S.H. Chue, Pressure probes for fluid measurement, Prog. Aero. Sci. 16 (No. 2) (1975) 147–223.
- [12] ISO 3966, Measurement of fluid flow in closed conduits — velocity area method using Pitot static tubes, ISO/TC 30/SC 5 Veloc, Mass Methods (2020).
- [13] ASTM, Standard Test Method for Average Velocity in a Duct (Pitot Tube Method), ASTM/D 3154-00, 2000.
- [14] ANSI/AMCA, Laboratory Methods of Testing Fans for Rating, AMCA 210, Int. Air Mov. Control Assoc., 1999.
- [15] J.I.S. B8330, Testing methods for tubor-fans, Japan Ind. Stand. Comm. (2000).
- [16] Y. Terao, M. van der Beek, T.T. Yeh, H. Müller, Final report on CIPM air speed key comparison (CCM-FF-K3), Metrologia 44 (2007).
- [17] N. Kurihara, Y. Terao, S.-I. Nakao, M. Takamoto, Uncertainty of laser Doppler velocimeter calibration for air speed standard, Trans. Japan Soc. Mech. Eng. Ser. B. 71 (2005).
- [18] A. Iwai, T. Funaki, N. Kurihara, Y. Terao, Y.M. Choi, New air speed calibration system at NMIJ for air speeds up to 90 m/s, Flow Meas, Instrumentalist 66 (2019) 132–140.
- [19] E. Ower, F.C. Johansen, On a determination of the pitot-static tube factor at low Reynolds numbers with special reference to the measurement of low air speed, Proc. Roy. Soc. Lond. A. 136 (1932).
- [20] S.G. Kandlikar, D. Schmitt, Characterization of surface roughness effects on pressure drop in single-phase flow in minichannels, Phys. Fluid. 17 (2005).
- [21] N.P. Mikhailova, E.U. Repik, Influence of viscosity on the readings of total-head tubes with small velocities of the flow, Izv. Akad. Nauk SSSR, Mekhainika Zhidkosti i Gaza. 1 (1976).
- [22] OIML R111-1, Weights of Classes E1, E2, F1, F2, M1, M1-2, M2, M2-3 and M3. Part 1: Metrological and Technical Requirements, OIML, 2004.
- [23] ISO, Guide to the Expression of Uncertainty in Measurement, vols. 98–3, ISO Guid, 2008.
- [24] M.G. Cox, The evaluation of key comparison data, Metrologia 39 (2002) 589.